Biomimetic Intelligence and Robotics 4 (2024) 100148

Contents lists available at ScienceDirect

Biomimetic Intelligence and Robotics

journal homepage: www.elsevier.com/locate/birob

Research Article

Locomotion control of a rigid-soft coupled snake robot in multiple environments

Xuanyi Zhou [a,b], Yuqiu Zhang [c], Zhiwei Qiu [a], Zhecheng Shan [a], Shibo Cai [a], Guanjun Bao [a,*]

[a] College of Mechanical Engineering, Zhejiang University of Technology, Hangzhou 310023, China
[b] State Key Laboratory of Chemical Engineering, College of Chemical and Biological Engineering, Zhejiang University, Hangzhou 310027, China
[c] College of Biomedical Science and Engineering, South China University of Technology, Guangzhou 510000, China

ARTICLE INFO

Article history:
Received 31 October 2023
Revised 3 February 2024
Accepted 14 February 2024
Available online 25 February 2024

Keywords:
Snake robot
Rigid–flexible coupled
Soft actuator
Motion gait analysis

ABSTRACT

The versatile motion capability of snake robots offers themselves robust adaptability in varieties of challenging environments where traditional robots may be incapacitated. This study reports a novel flexible snake robot featuring a rigid–flexible coupling structure and multiple motion gaits. To better understand the robot's behavior, a bending model for the soft actuator is established. Furthermore, a dynamic model is developed to map the relationship between the input air pressure and joint torque, which is the model base for controlling the robot effectively. Based on the wave motion generated by the joint coupling direction function in different planes, multiple motion gait planning methods of the snake-like robot are proposed. In order to evaluate the adaptability and maneuverability of the developed snake robot, extensive experiments were conducted in complex environments. The results demonstrate the robot's effectiveness in navigating through intricate settings, underscoring its potential for applications in various fields.

© 2024 The Author(s). Published by Elsevier B.V. on behalf of Shandong University. This is an open access article under the CC BY-NC-ND license (http://creativecommons.org/licenses/by-nc-nd/4.0/).

1. Introduction

Currently, robots have widespread applications in diverse fields such as security, search and rescue, transportation, et al. [1,2]. Operating in narrow and confined spaces is one of the practical requirement for robots in these domains, necessitating specialized capabilities like compact size and strong environmental adaptability [3]. Among all types of robots, snake robots have emerged as a focal point of research due to their multi-gait movement ability and adaptability to complex environments. Thus, researchers have long been engaged in the study of robots that can emulate snake-like motions.

In 1972, Hirose developed the first serpentine robot ACM-III that could move steadily over rough surfaces or winding paths due to its slender and flexible body [4]. Subsequently, Hirose conducted experimental studies on biological snakes, including detailed quantitative analyses of typical snake movement patterns [5]. Based on Hirose's groundbreaking work in both biological research methods and the development of snake robot prototypes [6–8], extensive theoretical and experimental investigations into snake robots have been conducted [9–11].

Biological snakes employ a variety of gaits to adeptly navigate ever-changing environmental conditions, inspiring the necessity for a diverse range of locomotion gaits in robotic snakes, a pivotal focus in snake robot research [12]. The most common biological snake gaits are lateral undulation gait, sidewinding gait, lateral roll gait and linear gait [13]. Biological snakes can autonomously employ the most suitable gait according to their surroundings and specific state. In different confined spaces, snakes can adopt various forms, such as approaching targets through linear movements during hunting, or employing sidewinding gait on loose sand [14]. Various serpentine robots, such as ACM-III [4], AmphiBot I/II [15] and Aiko [16], utilized a lateral wave gait for movement. While Modsnake [17] and Kulko [18] robots imitated the side-moving state of biological snakes. LocoSnake [19] and Graphene-Based snake robot [20] used accordion gait to explore narrow and restricted pipelines. Nevertheless, Bayraktaroglu's snake robot [21] realized efficient movement through linear gait. Various limb-free gaits offer valuable insights for the study of snake robot locomotion [5]. For example, modular climbing caterpillar robot [22], MMIR-V1/V2 [23] imitates the inchworm movement gait. And Chen designed a snake robot with Horizontal rolling gait [24]. Moreover, Hoshino proposed a snake robot to achieve jumping gait, thereby establishing the foundation for implementing jumping gaits in snake robots [25]. The snake robot Modsnake can realize three locomotion gaits: lateral movement, climbing and underwater swimming, which enables it to adapt to varied and rugged terrain [17]. And the lateral movement and lateral rolling gaits of Kulko enables itself to actively avoid obstacles [18]. Slim slime robot (SSR) can also realize three locomotion gaits: lateral wave, straight line and lateral roll, which enables it to traverse

* Corresponding author.
E-mail address: gjbao@zjut.edu.cn (G. Bao).

https://doi.org/10.1016/j.birob.2024.100148
2667-3797/© 2024 The Author(s). Published by Elsevier B.V. on behalf of Shandong University. This is an open access article under the CC BY-NC-ND license (http://creativecommons.org/licenses/by-nc-nd/4.0/).

complex terrain and operate in narrow Spaces [26]. It is obvious that Snake robots with multiple motion gaits often exhibit superior adaptability and maneuverability compared to those with a single motion gait, especially in complex environments. Thus, understanding the principle of various motion gaits in snake robots can certainly enhance their adaptability and maneuverability in complex environments.

A comprehensive investigation [13,15,27], including theoretical modeling, structural design, and control aspects of rigid snake robots, have shown that rigid snake robots can achieve efficient and stable motion across various terrains [17]. However, when compared to biological snakes, they still exhibit limitations in environmental adaptability. Biological snakes, with their soft bodies, demonstrate exceptional terrain navigation capabilities. The inherent softness enables them to traverse through narrow openings and adapt without causing harm to the environment or themselves [28]. With the advancement of flexible material technology, there is an opportunity to leverage the benefits of flexible materials to enhance the movement and environmental adaptability of snake robots. The pliability of flexible materials allows for the generation of more lifelike movements during the driving process, thereby significantly improving the environmental adaptability of snake robots. Additionally, the compact structure of flexible materials liberates snake robots from some intricate rigid structures, providing distinct advantages in navigating through restricted environments [29,30].

At present, there are several soft snake robots developed using flexible materials, including a compact snake robot with a length of only 0.185 m [31], a snake robot capable of maneuvering through narrow tubes [32], a versatile snake robot designed for various environments [33] and an underwater-swimming snake robot [34]. The operational environments and modes of movement of these soft snake robots closely resemble those of biological snakes, and some demonstrate adaptability to different surroundings. However, these soft snake robots are often tailored to specific scenarios, excelling in particular forms of movement within those defined contexts. When confronted with changing requirements or environments, there is a possibility that they may fail to produce effective movement [35]. While certain robotic snakes can perform movements in various environmental scenarios, it is essential to emphasize that this does not necessarily indicate genuine environmental adaptability in these soft snake robots.

In order to enhance environmental adaptability, a snake robot named "ZJUT Snake" is designed with a rigid–flexible coupling structure in this paper, enabling the execution of multiple motion gaits. The contributions of this work are summarized as follows:

(1) New mechanism and structure design of a soft-actuator-driven snake robot: The soft actuator enables flexible and stable movement, allowing the ZJUT Snake to achieve three-dimensional motion.

(2) Gait analysis method for snake robot Movement: In response to the diverse forms of snake robot movement, a gait analysis method is introduced. This method subdivides the movement gait into visual steps, analyzes the impact of each step on overall movement, and summarizes the rules governing the ZJUT Snake's attainment of various movement gaits. This lays the foundation for gait control.

(3) Realization of three locomotion gaits in the soft snake robot: Three distinct locomotion gaits were successfully implemented in the ZJUT Snake, validating its adaptability to environments with different gaits. This achievement enhances the ZJUT Snake's capability to navigate complex environments by employing multiple gaits.

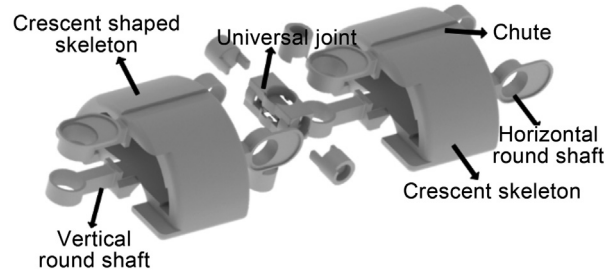

Fig. 1. Exploded view of rigid skeleton.

2. Structural design

The snake robot designed in this paper incorporates a novel concept of rigid-soft coupling, employing a modular design that integrates a rigid skeleton as its foundational structural unit and soft actuators as the propulsive driving component. The robot's dynamic motion is orchestrated by these soft actuators, synergizing the merits of both rigid and soft materials. This innovative combination enhances the structural strength and stability of the soft actuators, allowing the snake robot to maintain the flexibility and safety associated with soft robotics while also benefiting from the structural strength typically found in rigid robots.

2.1. Rigid skeleton structure

A rigid skeleton structure is proposed that can be installed inside a soft actuator, providing internal support to enhance the structural strength of the soft actuator. During the control of the soft actuator's motion, the inherent high flexibility and extensive degrees of freedom of the rigid skeleton ensure that it does not adversely affect the motion of the soft actuator. Additionally, by amounting sensors on the rigid skeleton, its motion state variables could be acquired. This approach facilitates the collection of motion data for soft materials, which is often challenging in soft robotics.

As shown in Fig. 1, the rigid skeleton structure is installed within the ten-chamber driving structure of the soft actuator. The overall rigid skeleton structure is composed of multiple crescent-shaped shells interconnected by universal joints. Vertical and horizontal round shafts are designed to facilitate the connection between crescent-shaped skeletal structures.

2.2. Soft actuator

The soft actuator, depicted in Fig. 2(a), comprises three primary components. The first part serves as a connection point and functions as the inflation inlet. External air pressure is introduced into the actuator through this inflation inlet, enabling control over the bending or elongation of the soft actuator in various directions. The second part consists of a ten-chamber driving unit, composed of ten pneumatic artificial muscles arranged in a specific geometric pattern, as illustrated in Fig. 2(b). The fundamental unit of the ten-chamber driving structure, the pneumatic artificial muscle, operates based on air pressure input. It is designed with an internal silicone core covered by an elastic polyester fabric. When air pressure is applied, the internal silicone expands and elongates, and constrained by the external polyester material, the pneumatic artificial muscle either elongates axially or expands radially. For this study, axial elongation-type pneumatic artificial muscles were utilized, extending axially with air pressure input.

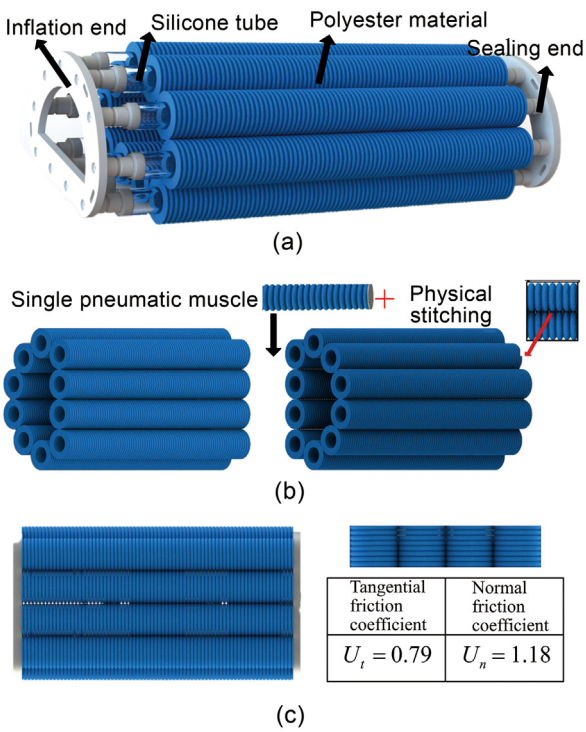

Fig. 2. Structure diagram of a snake robot. (a) Ten-cavity drive structure. (b) Ten cavities made of polyester. (c) Bottom of ten-cavity drive structure.

Upon inflating the ten-chamber driving structure, the coordinated action of the pneumatic artificial muscles induces a collective bending effect on the overall structure. The final component of the soft actuator serves as a connection point and fulfills a sealing function. This distinctive structural design of the soft actuator embodies three pivotal features: (1) Inflating the pneumatic artificial muscles empowers the soft actuator module to achieve motion in both horizontal and vertical directions, enabling the snake robot to execute three-dimensional gaits. (2) The bottom of the soft actuator introduces anisotropic friction. As the snake robot moves on the ground, it generates greater normal friction than tangential friction. This design allows the snake robot to traverse the ground, a critical element for generating forward propulsion in this soft snake robot. (3) The structural design of the soft actuator ensures exceptional mechanical stability. The flat bottom and elliptical body shape prevent the snake robot from tipping over during three-dimensional gaits, ensuring stability throughout its motion, even when swimming in water.

2.3. Motion principle of soft actuator

The mechanism of soft actuator elongation and bending induced by aerated artificial muscles is elucidated. Furthermore, we explore how precise control of air pressure input to the pneumatic artificial muscles enhances the soft actuator's capability to execute bends in both the horizontal and vertical planes.

The geometric configuration of the soft actuator is illustrated in Fig. 3(a), with A_1 to A_{10} representing ten pneumatic artificial muscles. Pneumatic artificial muscles A_1 to A_6 are arranged in a standard circular arc formation, with their centers oriented towards the geometric center O. Simultaneously, pneumatic artificial muscles A_7 to A_{10} are linearly distributed, with A_7 and A_{10} positioned externally and tangent to A_6 and A_1, respectively. The geometric centers of pneumatic artificial muscles A_7 and A_{10} are designated as points C and B, respectively.

Taking pneumatic artificial muscle A_3 as an example, we analyze the impact of a single pneumatic artificial muscle on the soft actuator after inflation. As depicted in Fig. 3(b), when air pressure is introduced into A_3, it experiences axial elongation. Structurally, A_2, A_3, and A_4 are mutually fixed tangentially. Consequently, when A_3 elongates axially, it stretches A_2 and A_4, causing them to move closer to one side of A_3. This stretching generates a tension force exerted by A_3 on A_2 and A_4, with the force directed towards A_3O.

Simultaneously inflating multiple pneumatic artificial muscles enables the attainment of bending in both the horizontal and vertical planes of the soft actuator. As illustrated in Fig. 3(c), when pneumatic artificial muscles A_1, A_2, and A_{10} are inflated concurrently, the directions of the forces acting on each pneumatic artificial muscle are as follows:

$$\overrightarrow{F_{A2}} = \cos\frac{\pi}{4}\cdot\vec{x} - \sin\frac{\pi}{4}\cdot\vec{y} \tag{1}$$

$$\overrightarrow{F_{A1}} = \cos\frac{\pi}{12}\cdot\vec{x} - \sin\frac{\pi}{12}\cdot\vec{y} \tag{2}$$

$$\overrightarrow{F_{A10}} = \cos\frac{11}{36}\pi\cdot\vec{x} + \sin\frac{11}{36}\pi\cdot\vec{y} \tag{3}$$

The direction of resultant F_1 is expressed as

$$\overrightarrow{F_1} = \overrightarrow{F_{A1}} + \overrightarrow{F_{A2}} + \overrightarrow{F_{A10}} = \left(\cos\frac{\pi}{12} + \cos\frac{\pi}{4} + \cos\frac{11\pi}{36}\right)\cdot\vec{x} + \left(\sin\frac{11\pi}{36} - \sin\frac{\pi}{12} - \sin\frac{\pi}{4}\right)\cdot\vec{y} \tag{4}$$

The inverse tangent function of $\overrightarrow{F_1}$ gives as $\arctan\overrightarrow{F_1} = -3.7°$. This also indicates that at this point, the angle between the direction of bending of the soft actuator and the X-axis is approximately $-3.7°$. To simplify the model of the soft actuator, we consider its motion under this inflation configuration as bending to the right. Due to the left–right symmetry in the structure of the soft actuator, when pneumatic artificial muscles A_5, A_6, and A_7 are simultaneously inflated, the direction of motion for the actuator is to the left. As shown in Fig. 3(d), when air pressure is injected into the pneumatic artificial muscles A_3 and A_4 at the same time:

$$\overrightarrow{F_{A3}} = \cos\frac{5}{12}\pi\cdot\vec{x} - \sin\frac{5}{12}\pi\cdot\vec{y} \tag{5}$$

$$\overrightarrow{F_{A4}} = \cos\frac{7}{12}\pi\cdot\vec{x} - \sin\frac{7}{12}\pi\cdot\vec{y} \tag{6}$$

The direction of the resultant F_2 is obtained by adding the two together:

$$\overrightarrow{F_2} = \overrightarrow{F_{A3}} + \overrightarrow{F_{A4}} = -2\sin\frac{5}{12}\pi\cdot\vec{y} \tag{7}$$

$\overrightarrow{F_2}$ has no X-direction component and is a negative value, which indicates that the soft actuator is bending in the opposite direction of the Y-axis, that is, bending down. As depicted in Fig. 2(e), when pneumatic artificial muscle A_8 and A_9 are charged with air pressure at the same time, the direction of $\overrightarrow{F_8}$ and $\overrightarrow{F_9}$ is pointing to the positive direction of the Y-axis, and the direction of the resultant force is also pointing to the Y-axis square, which indicates that the soft actuator is bending in the positive direction of the Y-axis at this time, that is, bending upward. Through these four inflation configurations involving multiple pneumatic artificial muscles, the soft actuator can achieve bending in both horizontal and vertical planes. If air pressure is simultaneously applied to the soft actuator to induce horizontal and vertical bending, the actuator will produce a combined effect of bending in both directions. When air pressure is simultaneously applied to all pneumatic artificial muscles, the soft actuator undergoes axial elongation. The bending effects of the soft actuator model are depicted in Fig. 4.

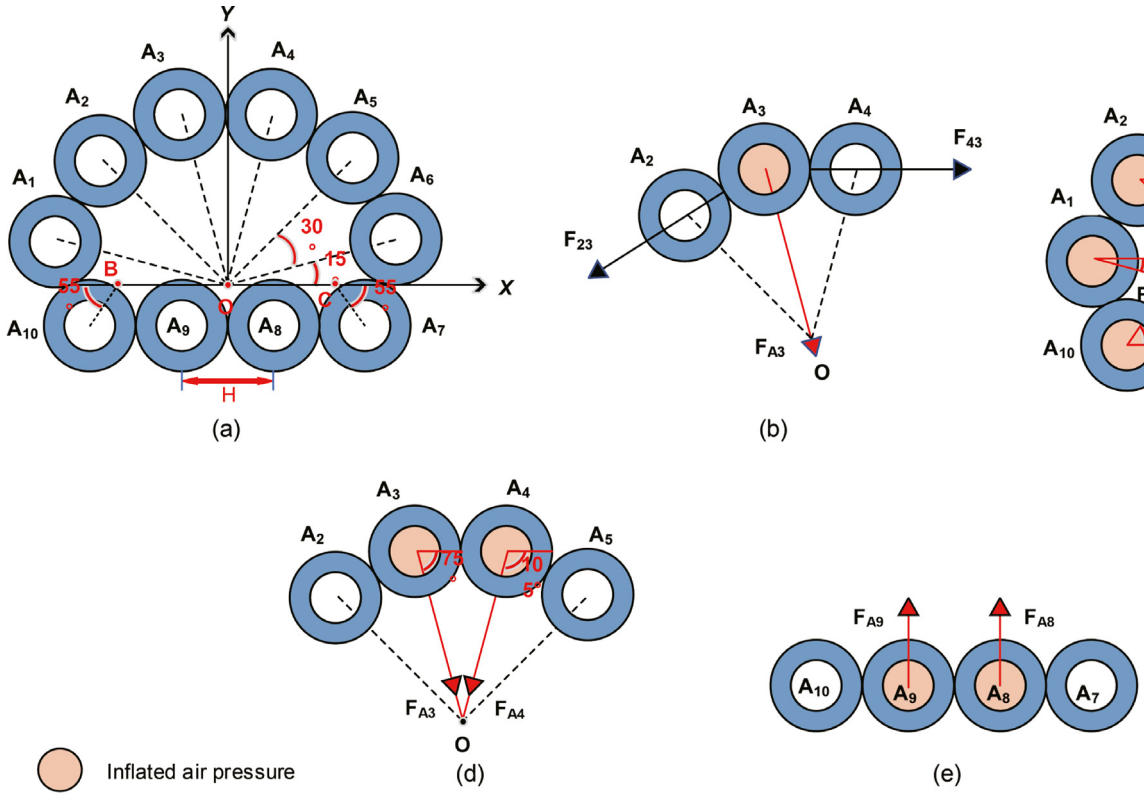

Fig. 3. Force analysis of soft actuator under different inflating modes.

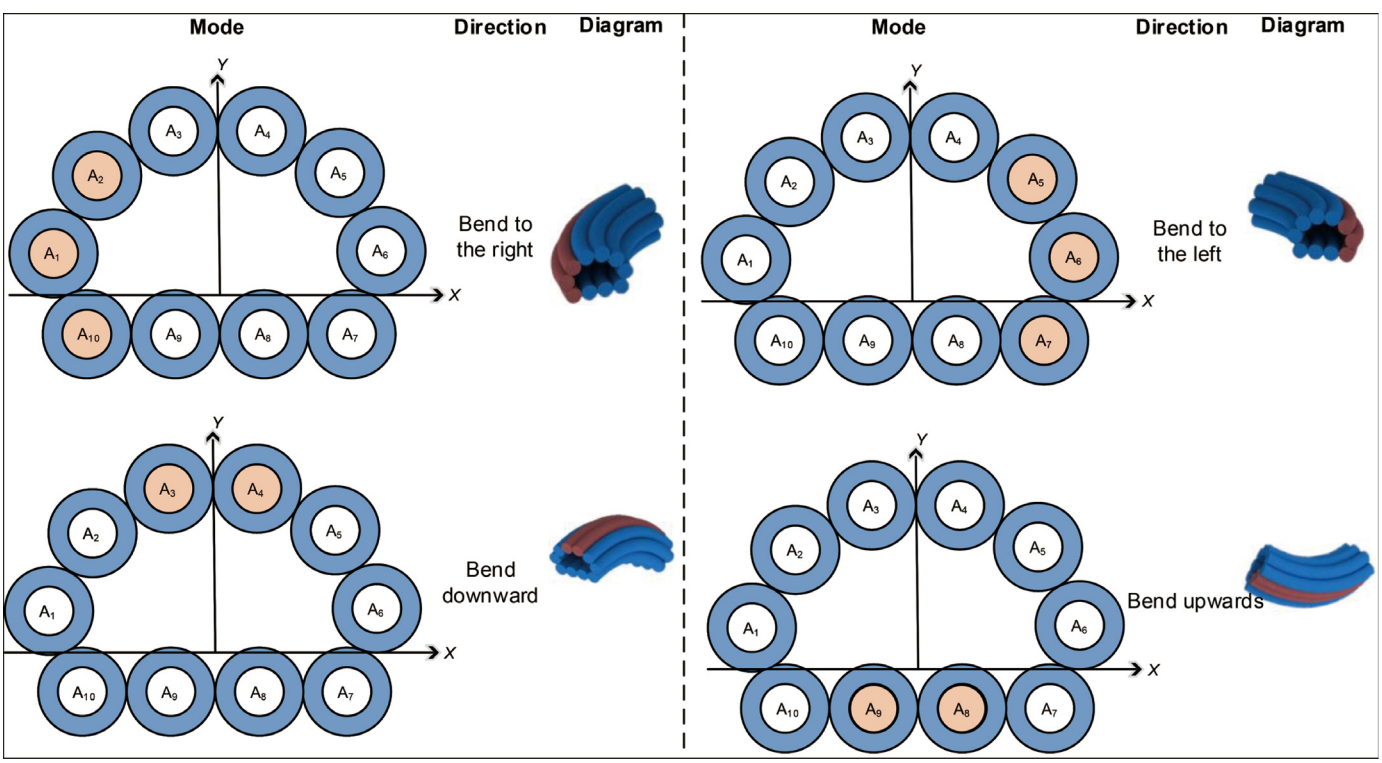

Fig. 4. The bending diagram of the soft actuator in four directions.

3. Locomotion control

By employing joint coupling direction functions to control the interconnected soft actuators on the snake robot, we achieved five distinct motion gaits: lateral undulation, sidewinding translation, lateral rolling, longitudinal traveling wave, and straight-line extension. Among these gaits, lateral undulation and longitudinal traveling waves are two-dimensional gaits occurring within one

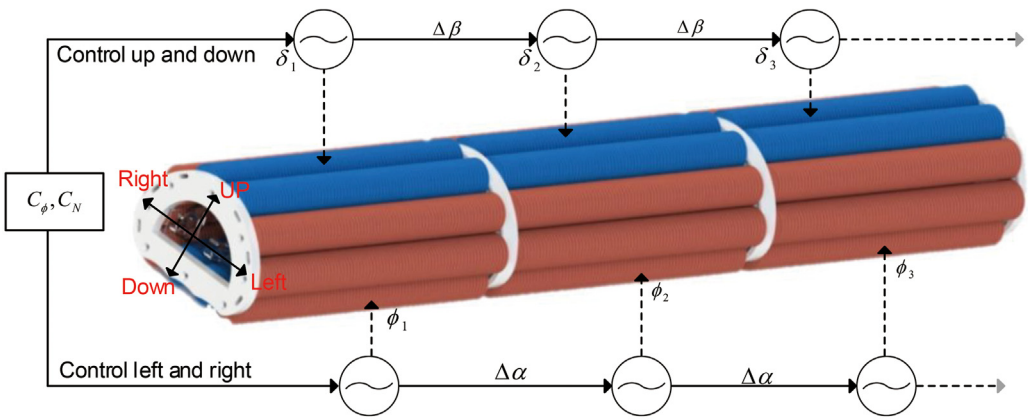

Fig. 5. Diagram of joint coupling function.

plane. Sidewinding translation, lateral rolling, and straight-line extension represent three-dimensional gaits, involving motion in two planes simultaneously. The diversity in the forms of these three-dimensional gaits liberates the snake robot's motion from environmental constraints, allowing it to adapt its gaits during movement according to the changing environment.

3.1. Joint coupling direction function

The control function in this paper is designed based on the Serpenoid control function for snake robot [36]. The control signals are generated in two orthogonal planes, as depicted in Fig. 5. The soft actuators serve as the driving joints of the snake robot, expressing them as functions of amplitude, period, offset, and phase in parameter space.

$$\begin{aligned} \phi_i &= D_\phi + A_\phi \sin(\frac{2\pi}{T_\phi} t + \alpha_0 - (i-1)\Delta\alpha) \\ \delta_i &= D_\delta + A_\delta \sin(\frac{2\pi}{T_\delta} t + \beta_0 - (i-1)\Delta\beta) \end{aligned} \tag{8}$$

where, joint yaw Angle ϕ_i is the left and right deflection angle of the joint driven by segment i in the horizontal direction, and joint pitch angle δ_i is the up and down deflection angle of the joint driven by segment i in the vertical direction. D, A and T in the joint coupling direction function represent offset, amplitude and period, respectively. α_0 and $\Delta\alpha$ represent the initial phase and phase lag of the drive joint in the direction of horizontal swing. β_0 and $\Delta\beta$ represent the initial phase and phase lag of the drive joint in the direction of vertical swing. The subscript i represents the joint position numbered from the head joint of the snake robot.

The positive or negative of the joint coupling direction function does not represent the size but the bending direction of the driving joint. When $\phi_i > 0$, the driving joint bends to the right in the horizontal direction; When $\phi_i < 0$, the driving joint bends to the left in the horizontal direction; When $\delta_i > 0$, the driving joint bends downward in the vertical direction; When $\delta_i < 0$, the driving joint bends upward in a vertical direction. Through the joint coupling direction function, we can control the snake robot to move in a specific manner in both the horizontal and vertical directions. The movement in these two directions is crucial for the snake robot's progression, as the interaction with the ground generates frictional forces that aid in its movement. The snake robot exhibits various gaits, and the roles of different parameters of the joint coupling direction function are described below.

Amplitude A: represents the maximum deflection angle of each drive joint in the horizontal or vertical direction, which varies from 0 to $\pi/2$. In a joint coupled direction function, it represents the degree of fluctuation (vertical or horizontal) of a segmented sine function.

Period T: determines the execution speed of the gait. During a gait cycle, all shapes (gestures) of any gait are performed in a continuous manner, after which the process is repeated.

Joint shift D: It will affect the direction of movement of the snake robot. When the average value of joint offset is 0, the snake robot will move in a straight line. When the average value of the joint offset is greater than 0, the snake robot will deflect counter-clockwise along the direction of motion. When the average value of the joint offset is less than 0, the snake robot will be deflected clockwise along the direction of motion.

Initial phase and phase lag: The initial phase affects the initial state of the sine wave, and the phase lag determines how the sine wave propagates along the snake robot, which can be stationary or propagated forward or backward.

3.2. Sidewinding state

This lateral motion gait is commonly employed by snakes residing in deserts or when encountering specific road conditions such as obstacles or unfavorable terrain. In this gait, the snake's interaction with the ground, achieved by swaying its body, aims not to move forward but rather to traverse sideways. To achieve the lateral motion gait, it is essential to control the snake robot to oscillate horizontally with a systematically changing yaw angle in the horizontal plane. Simultaneously, the pitch angle needs to be controlled to lift the snake robot's body off the ground periodically and adhere to the ground consistently in the vertical direction. When a specific joint of the snake robot moves horizontally in one direction, the joint is raised off the ground, generating a lateral offset. Conversely, when a particular joint moves horizontally in the opposite direction, it adheres to the ground, increasing friction, thus minimizing or eliminating the lateral offset. The joint coupling direction function under the lateral motion gait is expressed as

$$\phi_i = \frac{1}{3}\pi \sin(\frac{2\pi}{12} t + (i-1)\frac{1}{3}\pi) \tag{9}$$

$$\delta_i = \frac{1}{9}\pi \sin(\frac{2\pi}{12} t + \frac{\pi}{2} + (i-1)\frac{2}{3}\pi) \tag{10}$$

Utilizing joint coupling direction functions, the gait diagram for the snake robot's sidewinding locomotion is depicted in Fig. 6. The sidewinding gait is segmented into six steps (excluding the initial state and the subsequent gait cycle), where steps 1 to 6 collectively form one gait cycle. In the sidewinding locomotion gait, the snake robot, with its tail joint or head joint making

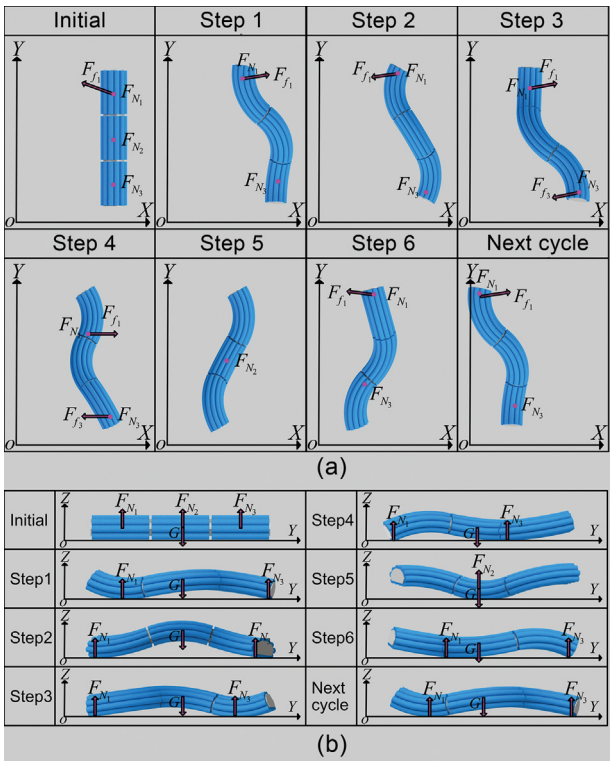

Fig. 6. The steps of sidewinding gait. (a) Top view of lateral roll gait. (b) Right view of lateral roll gait.

contact and adhering to the ground, utilizes the middle joint to propel the head joint in a specific direction. This mechanism enables the snake robot to maintain fixation of its tail segment while facilitating movement of the middle and head segments. Subsequently, the snake robot adjusts its posture to achieve fixation of the head segment while permitting movement of the middle and tail segments.

From the initial state to step 2: The snake robot's tail joint bends upward to adhere to the ground, maintaining a fixed position with slight deviations. The middle joint bends downward to lift off the ground, while driving the head joint to the left, enabling the snake robot to move in that direction.

From step 2 to step 3: This is a transitional pose change. The snake robot adjusts its head joint by bending it upward to adhere to the ground, and the middle and tail joints bend downward, preparing for the subsequent tail movement.

From step 3 to step 5: The snake robot's head joint remains fixed with slight deviations. The middle joint drives the tail joint to bend to the left, causing this portion of the snake robot to move leftward.

From step 5 to step 6: This is another transitional pose change. The snake robot adjusts its posture in preparation for head segment movement.

At this point, the snake robot completes a full cycle of sidewinding locomotion involving head movement, tail movement, and two transitional posture adjustments. By continuously repeating steps 1 to 6, the snake robot can achieve uninterrupted sidewinding movement. In the side-moving state, the robot and the ground also produce various opposite friction forces:

$$\begin{pmatrix} F_{f_i,x} \\ F_{f_i,y} \end{pmatrix} = -\begin{pmatrix} U_t(\cos\phi_i)^2 + U_n(\sin\phi_i)^2 & (U_t - U_n)\cos\phi_i\sin\phi_i \\ (U_t - U_n)\cos\phi_i\sin\phi_i & U_t(\sin\phi_i)^2 + U_n(\cos\phi_i)^2 \end{pmatrix}\begin{pmatrix} \dot{X}_{f_i} \\ \dot{Y}_{f_i} \end{pmatrix} \tag{11}$$

where U_t is the friction coefficient in the tangential direction, U_n is the friction coefficient in the normal direction, X_f and Y_f represent the velocity at the center coordinate of the ith joint.

$$F_{f_1,x} + F_{f_2,x} + F_{f_3,x} = M\ddot{X}_G \tag{12}$$

$$F_{f_1,y} + F_{f_2,y} + F_{f_3,y} = M\ddot{Y}_G \tag{13}$$

where X_G and Y_G are the acceleration of the robot's centroid coordinates.

3.3. Rolling gait

The rolling motion is a composite gait that amalgamates both horizontal and vertical movements of the snake robot, enabling it to maneuver flexibly in two orthogonal planes: horizontal and vertical. In this gait, the snake robot's roll and pitch angles undergo periodic sinusoidal oscillations. The snake robot consistently bends in a specific direction, leading to interaction forces between the driving joints and the ground. These interaction forces generate torque, initiating the rolling motion. Through the lateral rolling gait, the snake robot can execute sideward rolling and surmount certain ground obstacles. In the lateral rolling gait, the joint coupling direction functions are outlined as follows:

$$\phi_i = \frac{1}{6}\pi \sin\frac{2\pi}{12}t \tag{14}$$

$$\delta_i = \frac{1}{4}\pi \sin(\frac{2\pi}{12}t + \frac{1}{2}\pi) \tag{15}$$

Through joint coupling direction functions, the stages of the rolling gait are depicted in Fig. 7. The rolling gaits consist of eight steps (excluding the initial state and the subsequent cycle gait), with steps 1 to 8 constituting one cycle of lateral rolling gait. In the lateral rolling gait, the snake robot bends itself in one direction, enhancing ground support by flexing the driving joints toward the ground. Consequently, this motion induces the snake robot to perform a roll. Here is a step-by-step breakdown.

From the initial state to step 1: All driving joints of the snake robot bend to the left. The direction of the frictional force opposes the movement direction of the driving joints.

From step 1 to step 2: All driving joints bend downward. As the snake robot is in a left-bent position, the ground support forces F_{N1}, F_{N2}, and F_{N3} do not align on the same line. The robot experiences a clockwise torque. When the middle joint briefly lifts off the ground, the robot is only supported by F_{N1} and F_{N3}, and the torque reaches its maximum. When the torque is significant enough, the robot flips clockwise. After a certain angle, the middle joint recontacts the ground, and the head and tail joints lift off, achieving a momentary balance.

From step 2 to step 3: The snake robot gradually returns from the left-bent position to a straight line but increases its downward bending angle. In the Step 3 view of Fig. 7, the snake robot increases its leftward bending amplitude and the head and tail joints no longer lift off, returning to contact with the ground and preparing for the next flip action.

From step 3 to step 4: The snake robot bends to the right. In the Step 3 view of Fig. 7, the robot is bending toward the ground, and this bending generates a clockwise torque, driving the robot to flip clockwise.

From step 4 to step 5: The snake robot gradually returns from the downward bent position to a straight line and begins bending to the right. In the step 5 view of Fig. 7, the robot resumes ground contact and bends to the left, preparing for the next flip action.

From step 5 to step 6: The snake robot bends upward. In the step 5 view of Fig. 7 the robot bends toward the ground, and this bending generates a torque that drives the robot to flip clockwise.

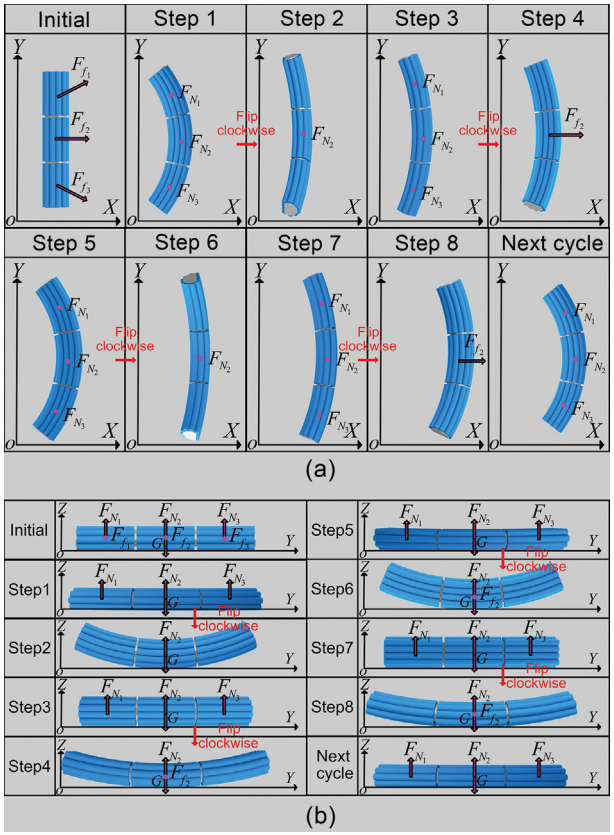

Fig. 7. Steps of rolling gait.

From step 6 to step 7: The snake robot gradually returns from the right-bent position to a straight line and increases its upward bending angle. In the step 7 view of Fig. 7, the robot resumes ground contact and increases its leftward bending angle, preparing for the next flip action.

Finally, from step 7 to step 8: The snake robot bends to the left. In the step 7 view of Fig. 7, the robot bends toward the ground, generating a torque that drives the robot to flip clockwise. At this point, the robot completes one full cycle of lateral rolling gait, having performed a full clockwise rotation. In the next cycle, the robot repeats these steps continuously to achieve the lateral rolling gait.

In the rolling gait, various external forces act on the robot. These include gravity (G), ground support force (F_N), and ground friction force (F_f). During several steps of the robot's flipping motion, the robot experiences a balance between the support force and gravity. Due to the symmetrical relationship between the support forces F_{N1} and F_{N3}, at this point.

$$F_{N_1} = F_{N_3} = \frac{1}{4}G \tag{16}$$

$$F_{N_2} = \frac{1}{2}G \tag{17}$$

The torque M of the robot is

$$M = \frac{1}{2}(X_{N_2} - X_{N_1})G \tag{18}$$

When the middle joint of the robot lifts off the ground, it is solely acted upon by the support forces F_{N1} and F_{N3}. At this moment, the robot experiences the maximum torque, denoted as M_{max}.

$$F_{N_1}{}' = F_{N_3}{}' = \frac{1}{2}G \tag{19}$$

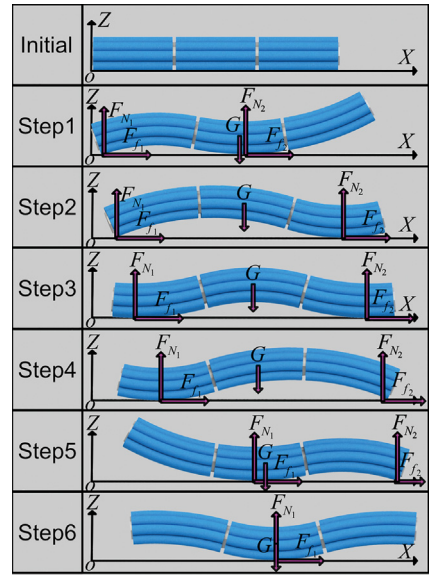

Fig. 8. Right view of longitudinal traveling wave gait steps.

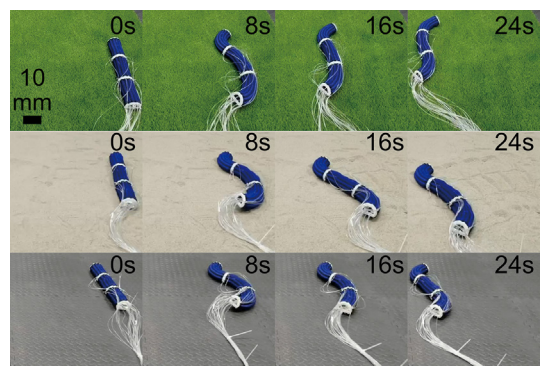

Fig. 9. Sidewinding-step in three scenarios.

$$M_{\max} = (X_G - X_{N_1})G \tag{20}$$

3.4. Longitudinal traveling wave gait

The longitudinal traveling wave gait is another locomotion pattern employed by snake robots. In terms of motion, it adapts the lateral wave motion gait to the vertical plane, requiring less space for movement, making it well-suited for narrow and constrained environments. In this gait, it is essential to control the pitch angle of the snake robot to generate a forward-propagating sine wave, enabling the robot to execute regular swings in the vertical plane. The joint coupling direction function for the longitudinal traveling wave gait is as follows:

$$\delta_i = \frac{1}{2}\pi + \frac{2}{3}\pi \sin(\frac{2\pi}{12}t + (i-1)\frac{2}{3}\pi) \tag{21}$$

Through the joint coupling direction function, the steps of longitudinal traveling wave gait are shown in Fig. 8. The longitudinal traveling wave gait has 6 steps, excluding the robot's initial state. During the longitudinal traveling wave gait, the snake robot transforms its body shape into a continuously propagating sine wave in the vertical plane. It achieves this by generating rolling friction with the ground at the bottom of each joint, propelling itself forward.

From the initial state to step 1, the snake robot raises its head joint and uses the friction between the middle joint and

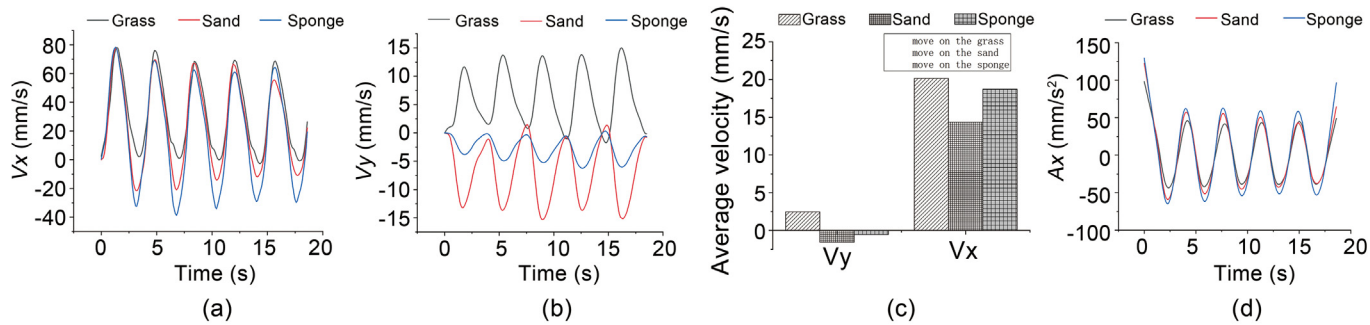

Fig. 10. Motion state of sidewinding.

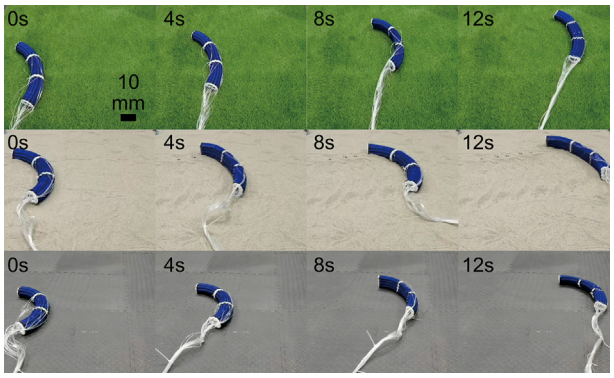

Fig. 11. Rolling gait in three scenarios.

the ground to generate forward propulsion. The tail joint only supports the ground, providing balance.

From step 1 to step 2, the snake robot lifts the middle joint and uses the friction between the head joint and the ground for propulsion. At this stage, the tail joint still serves to maintain balance.

From step 2 to step 3, the robot simultaneously contacts the ground with both the tail joint and the head joint, creating friction for self-propulsion.

From step 3 to step 4, the robot generates propulsion through the friction between the tail joint and the ground, while the head joint supports the ground to maintain balance.

From step 4 to step 5, the robot uses the friction between the middle joint and the ground for propulsion.

From step 5 to step 6, the robot adjusts its posture, keeping the middle joint in contact with the ground and lifting both the head and tail joints off the ground, smoothly transitioning to the next gait cycle.

The external forces applied to the robot under the longitudinal traveling wave gait are gravity G, ground support force F_N and ground friction force F_f, respectively. Gravity and support force are balanced, and the combined force of the robot is friction force. Therefore, friction force is the driving force of the robot, and the balance of force and torque can be obtained:

$$F_{N_1} = (G + M\ddot{Z}_G)\frac{X_{N_2} - X_G}{X_{N_2} - X_{N_1}} + M\ddot{X}_G\frac{Z_G}{X_{N_2} - X_{N_1}} \tag{22}$$

$$F_{N_2} = G - F_{N_1} \tag{23}$$

where M is the mass of the robot, the position of the centroid coordinates of the robots X_G and Z_G under the XOZ plane, MX_G and MZ_G are the inertial forces of the robot along the X and Z axes, X_{N1} and X_{N2} are the X-axis coordinates of the supporting forces F_{N1} and F_{N2}, and the magnitude of friction is $F_{Ni} = U_N F_{Ni}$, where the friction coefficient U_N is the normal friction coefficient.

Table 1
Three environmental scenarios.

Material	Friction coefficients (with robot)	Size (m)	Depth (mm)
Grass	$U_t = 0.79, U_n = 1.18$	$4 * 3$	8
Sand	$U_t = 0.47, U_n = 0.71$	$3 * 2$	5
Sponge	$U_t = 0.91, U_n = 1.03$	$3 * 3$	10

4. Experiments

Three environmental scenarios were designed to assess the movement of the snake robot. These scenarios represent two outdoor environments, namely grassy terrain and sandy terrain, and one indoor environment characterized by a foam mat surface. During the experiments, markers were affixed to the snake robot, and an external vision system, NOKOV, was employed to record the data of motion. The results indicated that although there were some variations in the performance of these five gaits across different environmental scenarios, the snake robot's motion was not significantly impacted by changes in the environment. The robot demonstrated effective adaptability to each scenario as shown in Table 1.

4.1. Sidewinding experiment

The experimental results of the sidewinding state are presented in Fig. 10, depicting the snake robot's motion across three environmental scenes: grass, sand, and a sponge mat (shown in Fig. 9). In this gait, the primary movement of the snake robot involves lateral displacement along the X-axis, with a minor displacement in the Y-axis direction. However, the fluctuation amplitude of Vx significantly surpasses that of Vy. The snake robots exhibit swift sideways motion, characterized by high-speed gaits. The average speeds of Vx on grassland, sand, and the sponge mat were 20.15 mm/s, 14.35 mm/s, and 18.74 mm/s, respectively, while the average speeds of Vy on grassland, sand, and the sponge mat were 2.48 mm/s, −1.55 mm/s, and −0.53 mm/s, respectively. The acceleration of the snake robot in the Y direction was utilized to calculate the frictional force acting on the snake robot.

4.2. Rolling experiment

In the rolling experiments depicted in Fig. 11, the snake robot's motion state is recorded in Fig. 12 across three distinct environmental surfaces: grass, sand, and foam mats. During the rolling gait, one side of the snake robot contacted with the ground and acted as the pivot axis for the rolling motion. The characteristics of rolling motion on grass, sand, and foam mats exhibit similarities, with the lateral rolling gait primarily relying on ground reaction forces and experiencing minimal influence from

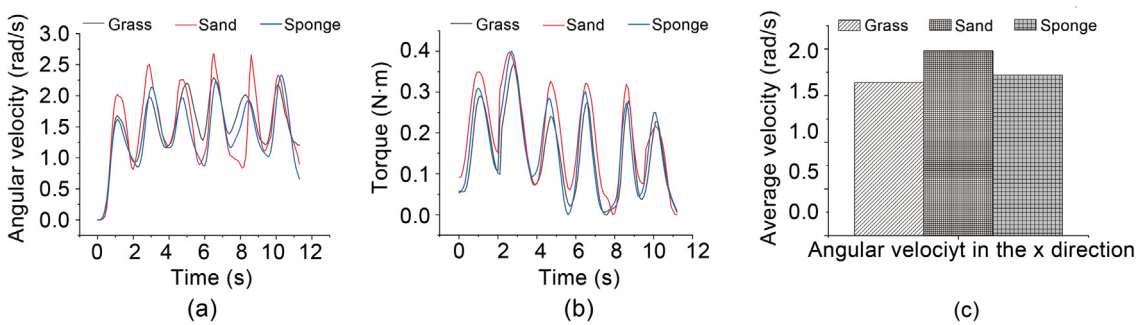

Fig. 12. Motion state of rolling.

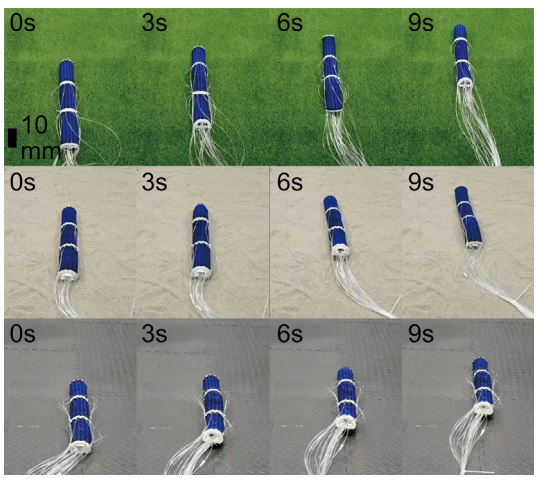

Fig. 13. Longitudinal traveling wave gait in three scenarios.

friction. The average rolling velocities of the snake robot on grass, sand, and foam mats are 1.64 rad/s, 1.98 rad/s, and 1.72 rad/s, respectively. Additionally, we computed the torque generated by the snake robot during lateral rolling gait based on its angular acceleration.

4.3. Longitudinal traveling wave experiment

In the longitudinal traveling wave gait experiment shown in Fig. 13, the motion state of the snake robot is recorded in Fig. 14 across three environmental scenarios: grass, sand, and sponge mat. In the longitudinal traveling wave gait, the snake robot exhibits inchworm-like motion along the Y-axis, with its motion speed fluctuating in tandem with the stretching frequency of the inchworm motion. Notably, on sand, the snake robot's speed in the longitudinal traveling wave decreases progressively due to the reduced friction coefficient as it moves and displaces sand. The average moving speed of the snake robot on grass, sand, and foam mats was 7.74 mm/s, 2.7 mm/s, and 5.14 mm/s, respectively. Additionally, we computed the force of friction acting on the snake robot in the Y direction based on the robot's acceleration.

4.4. Gait movement characteristics

The distinctive characteristics of these five gaits are summarized as follows:

Sidewinding Gait: This gait allows lateral movement while introducing some forward and backward displacement. It is characterized by rapid lateral motion, and when faced with obstacles, its ability to navigate around them passively is facilitated by the combined lateral and longitudinal movements.

Rolling Gait: The lateral rolling gait involves lateral axial rolling and requires a relatively large motion space. When confronted with obstacles, it can actively overcome them by rolling over, and it relies on ground reaction forces, resulting in minimal impact from environmental changes.

Longitudinal traveling: This gait imitates inchworm-like movement, enabling slow but efficient forward and backward motion. It requires less spatial clearance and can navigate through narrow environments.

These characteristics provide a comprehensive understanding of the adaptability and utility of each gait in different scenarios and environments.

4.5. Complex environments

Finally, we conducted experiments with the snake robot in a complex environment, as illustrated in Fig. 15. This intricate setting encompassed grassy terrain, wooden stick obstacles (0.5 m in length and 12.5 mm in diameter), narrow pipe passages (inner diameter of 100 mm), sandy terrain, and a straight track scene. This experimental arrangement emulates the challenging

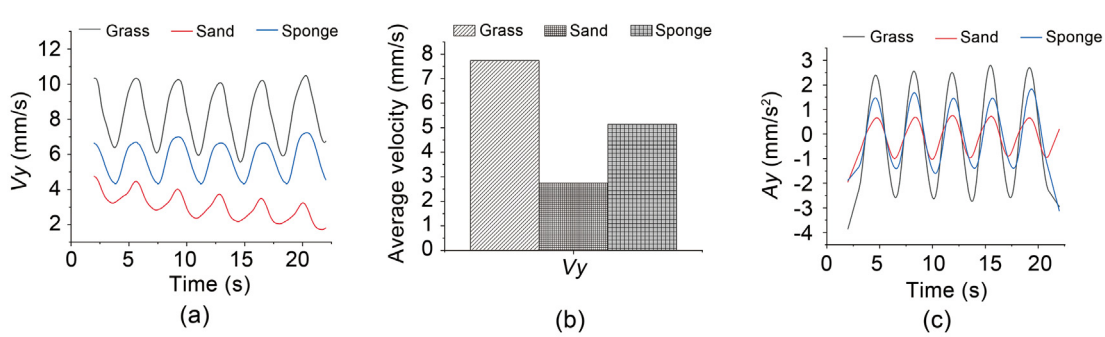

Fig. 14. Motion state of longitudinal traveling wave.

Fig. 15. Complex environments of the snake robot.

outdoor environments typical of real snakes. Moreover, the scenarios underwent frequent changes, requiring the snake robot to demonstrate a diverse range of locomotion capabilities to navigate environmental shifts.

In the initial 30 s, the snake robot employs the lateral wave gait as it navigates through the grass scene, eventually reaching the stick obstacle scene. Encountering an obstruction at the front, the snake robot, between 40 and 70 s, transitions to lateral movement gait, repositioning itself to the lower-left side of the stick obstacle scene. Subsequently, the snake robot adjusts its posture and executes the rolling gait to surmount these obstacles. After 15 s, the snake robot successfully conquers the stick obstacles, progressing to the narrow pipeline scene in 1 min and 30 s. In the narrow pipe scene, characterized by limited entrance space, the snake robot, from 1 min and 55 s to 2 min and 55 s, approaches and enters the narrow pipe using straight-line motion with a longitudinal traveling wave gait. Although confined within the narrow pipe, the longitudinal traveling wave gait allows the snake robot to generate propulsive force by rubbing against the inner wall. After sustaining this motion for a period, the snake robot successfully traverses the narrow pipe, arriving at the sandy scene by 8 min and 50 s. Between 9 min and 30 s and 10 min, the snake robot approaches the linear orbit scene using lateral moving gait. Due to most of the snake robot's body remaining in the narrow pipe, resulting in minimal tail displacement during lateral movement, the snake robot extends its tail through the narrow pipe in the sand scene between 10 and 10 min and 30 s. From 10 min and 30 s to 10 min and 50 s, the snake robot executes lateral tumbling gait as it approaches the linear track scene. Between 10 min and 50 s and 12 min and 30 s, the snake robot adjusts its posture using both the longitudinal traveling wave gait and lateral moving gait until it enters the straight track. From 13 min and 10 s to 17 min and 40 s, the snake robot first enters the linear orbit using longitudinal traveling wave gait and then departs from

the linear orbit through linear stretching gait. By 20 min and 40 s, the snake robot is on the verge of completely leaving the straight track, providing ample space for other gaits. At this point, around 21 min, the snake robot executes a lateral rolling gait and flips over the straight track. Ultimately, after 21 min, the snake robot successfully completes the traversal of the entire complex environment.

Throughout the experiment, the snake robot adeptly adjusts its motion gait in response to diverse environmental scenes, showcasing its capability to modulate spatial positioning through a repertoire of moving gaits. This underscores the advantages of a snake robot equipped with multiple locomotion gaits, emphasizing its adaptability and agility in navigating complex environments.

5. Conclusion

To enhance the locomotion and environmental adaptability of the snake-like robot, we introduced a soft-bodied snake robot featuring a diverse range of locomotion gaits. Comprising three interconnected soft actuators representing the head, body, and tail segments, this robot incorporates radially arranged pneumatic artificial muscles at the bottom of each soft actuator. This design introduces anisotropic friction during motion, and enabling versatile movement. The soft actuators exhibit flexibility in both horizontal and vertical directions, along with radial extension, forming the basis for three-dimensional gaits in the snake robot.

The developed robot showcases an extended range of locomotion patterns, surpassing the capabilities of previous single-mode robots [37,38]. It seamlessly executes sidewinding, rolling, and longitudinal traveling wave motions, significantly enhancing its adaptability to diverse environments. Whether maneuvering through regular grassy terrain, traversing loose sandy ground, or gliding across soft sponge padding, the robot excels with these three locomotion modes. Noteworthy is the robot's exceptional performance in complex environments, where it adeptly overcomes obstacles, navigates narrow passages, and operates efficiently in confined spaces. The developed soft-bodied snake robot demonstrated its motion capability and adaptability across a wide spectrum of environments.

Declaration of competing interest

The authors declare that they have no known competing financial interests or personal relationships that could have appeared to influence the work reported in this paper.

Acknowledgments

This research was financially supported by the Joint Fund of National Natural Science Foundation of China with Shenzhen City (U2013212) and the National Key R&D Program of China (2020YFB1313001).

Appendix A. Supplementary data

Supplementary material related to this article can be found online at https://doi.org/10.1016/j.birob.2024.100148.

References

[1] J. Casper, R.R. Murphy, Human–robot interactions during the robot-assisted urban search and rescue response at the World Trade Center, IEEE Trans. Syst. Man Cybern. B 33 (3) (2003) 367–385.
[2] F. Rubio, F. Valero, C. Llopis-Albert, A review of mobile robots: Concepts, methods, theoretical framework, and applications, Int. J. Adv. Robot. Syst. 16 (2) (2019) 1729881419839596.
[3] W. Huang, Z. Xu, J. Xiao, W. Hu, H. Huang, F. Zhou, Multimodal soft robot for complex environments using bionic omnidirectional bending actuator, IEEE Access 8 (2020) 193827–193844.
[4] S. Hirose, Biologically inspired robots, Snake-Like Locomot. Manip. (1993).
[5] Z.Y. Bayraktaroglu, Snake-like locomotion: Experimentations with a biologically inspired wheel-less snake robot, Mech. Mach. Theory 44 (3) (2009) 591–602.
[6] M. Mori, S. Hirose, Development of active cord mechanism ACM-R3 with agile 3D mobility, in: Proceedings 2001 IEEE/RSJ International Conference on Intelligent Robots and Systems. Expanding the Societal Role of Robotics in the Next Millennium (Cat. No. 01CH37180), 2001, pp. 1552–1557.
[7] M. Mori, S. Hirose, Three-dimensional serpentine motion and lateral rolling by active cord mechanism ACM-R3, in: IEEE/RSJ International Conference on Intelligent Robots and Systems, 2002, pp. 829–834.
[8] S. Hirose, F. Matsuno, Development of snake robots for rescue operation design of the shape and its control, J. Jpn. Soc. Mech. Eng. 106 (1019) (2003) 769–773.
[9] G.S. Chirikjian, Theory and Applications of Hyper-Redundant Robotic Manipulators, California Institute of Technology, 1992.
[10] G.S. Chirikjian, J.W. Burdick, The kinematics of hyper-redundant robot locomotion, IEEE Trans. Robot. Autom. 11 (6) (1995) 781–793.
[11] J. Ostrowski, J. Burdick, Geometric Perspectives on the Mechanics and Control of Robotic Locomotion, Robotics Research, Springer, 1996, pp. 536–547.
[12] A. Maity, S. Majumder, Implementation of serpentine locomotion, Int. J. Intell. Syst. Technol. Appl. 11 (1–2) (2012) 81–101.
[13] P. Liljebäck, K.Y. Pettersen, Ø. Stavdahl, J.T. Gravdahl, Snake Robots: Modelling, Mechatronics, and Control, Springer, 2013.
[14] J. Liu, Y. Tong, J. Liu, Review of snake robots in constrained environments, Robot. Auton. Syst. 141 (2021) 103785.
[15] J.K. Hopkins, B.W. Spranklin, S.K. Gupta, A survey of snake-inspired robot designs, Bioinspiration Biomim. 4 (2) (2009) 021001.
[16] A.A. Transeth, P. Liljeback, K.Y. Pettersen, Snake robot obstacle aided locomotion: An experimental validation of a non-smooth modeling approach, in: 2007 IEEE/RSJ International Conference on Intelligent Robots and Systems, 2007, pp. 2582–2589.
[17] C. Wright, A. Johnson, A. Peck, Z. Mccord, A. Naaktgeboren, P. Gianfortoni, M. Gonzalez-Rivero, R. Hatton, H. Choset, Design of a modular snake robot, in: 2007 IEEE/RSJ International Conference on Intelligent Robots and Systems, 2007, pp. 2609–2614.
[18] P. Liljebäck, K.Y. Pettersen, Ø. Stavdahl, J.T. Gravdahl, A hybrid model of obstacle-aided snake robot locomotion, in: 2010 IEEE International Conference on Robotics and Automation, 2010, pp. 675–682.
[19] I. Virgala, M. Dovica, M. Kelemen, E. Prada, Z. Bobovský, Snake robot movement in the pipe using concertina locomotion, Appl. Mech. Mater. (2014) 121–129.
[20] Y. Yang, M. Zhang, D. Li, Y. Shen, Graphene-based light-driven soft robot with snake-inspired concertina and serpentine locomotion, Adv. Mater. Technol. 4 (1) (2019) 1800366.
[21] Z.Y. Bayraktaroglu, A. Kilicarslan, A. Kuzucu, V. Hugel, P. Blazevic, Design and control of biologically inspired wheel-less snake-like robot, in: The First IEEE/RAS-EMBS International Conference on Biomedical Robotics and Biomechatronics, 2006. BioRob 2006, 2006, pp. 1001–1006.
[22] W. Wang, K. Wang, H. Zhang, Crawling gait realization of the mini-modular climbing caterpillar robot, Prog. Natl. Sci. 19 (12) (2009) 1821–1829.
[23] W. Saab, P. Racioppo, A. Kumar, P. Ben-Tzvi, Design of a miniature modular inchworm robot with an anisotropic friction skin, Robotica 37 (3) (2019) 521–538.
[24] L. Chen, Y. Wang, S. Ma, B. Li, Studies on lateral rolling locomotion of a snake robot, in: IEEE International Conference on Robotics and Automation, 2004. Proceedings. ICRA'04, vol. 2004, 2004, pp. 5070–5074.
[25] K. Hoshino, M. Tanaka, F. Matsuno, Optimal shape of a snake robot for jumping, in: 2010 IEEE International Conference on Robotics and Automation, 2010, pp. 697–702.
[26] H. Ohno, S. Hirose, Study on slime robot (proposal of slime robot and design of slim slime robot), in: Proceedings. 2000 IEEE/RSJ International Conference on Intelligent Robots and Systems (IROS 2000)(Cat. No. 00CH37113), 2000, pp. 2218–2223.
[27] F. Sanfilippo, J. Azpiazu, G. Marafioti, A.A. Transeth, Ø. Stavdahl, P. Liljebäck, Perception-driven obstacle-aided locomotion for snake robots: the state of the art, challenges and possibilities, Appl. Sci. 7 (4) (2017) 336.

[28] I. Erkmen, A.M. Erkmen, F. Matsuno, R. Chatterjee, T. Kamegawa, Snake robots to the rescue!, IEEE Robot. Autom. Mag. 9 (3) (2002) 17–25.
[29] Y. Yang, Y. Wu, C. Li, X. Yang, W. Chen, Flexible actuators for soft robotics, Adv. Intell. Syst. 2 (1) (2020) 1900077.
[30] B. Zhang, Y. Fan, P. Yang, T. Cao, H. Liao, Worm-like soft robot for complicated tubular environments, Soft Robot. 6 (3) (2019) 399–413.
[31] M. Luo, M. Agheli, C.D. Onal, Theoretical modeling and experimental analysis of a pressure-operated soft robotic snake, Soft Robot. 1 (2) (2014) 136–146.
[32] X. Qi, H. Shi, T. Pinto, X. Tan, A novel pneumatic soft snake robot using traveling-wave locomotion in constrained environments, IEEE Robot. Autom. Lett. 5 (2) (2020) 1610–1617.
[33] C. Branyan, Y. Menğüç, Soft snake robots: Investigating the effects of gait parameters on locomotion in complex terrains, in: 2018 IEEE/RSJ International Conference on Intelligent Robots and Systems, IROS, 2018, pp. 1–9.
[34] H. Feng, Y. Sun, P.A. Todd, H.P. Lee, Body wave generation for anguilliform locomotion using a fiber-reinforced soft fluidic elastomer actuator array toward the development of the eel-inspired underwater soft robot, Soft Robot. 7 (2) (2020) 233–250.
[35] M. Calisti, G. Picardi, C. Laschi, Fundamentals of soft robot locomotion, J. R. Soc. Interface 14 (130) (2017) 20170101.
[36] D. Li, C. Wang, H. Deng, Y. Wei, Motion planning algorithm of a multi-joint snake-like robot based on improved serpenoid curve, IEEE Access 8 (2020) 8346–8360.
[37] P. Liljeback, K.Y. Pettersen, Ø. Stavdahl, J.T. Gravdahl, Snake robot locomotion in environments with obstacles, IEEE/ASME Trans. Mechatronics 17 (6) (2011) 1158–1169.
[38] M. Luo, R. Yan, Z. Wan, Y. Qin, J. Santoso, E.H. Skorina, Onal C.D., Orisnake: design, fabrication, and experimental analysis of a 3-D origami snake robot, IEEE Robot. Autom. Lett. 3 (3) (2018) 1993–1999.